Table 2

Baseline Characteristics and Previous Treatments of the Overall Population Included in the Final Analysis

Parameter	Value*
Baseline clinical characteristics ($n = 43$)†	
Hemoglobin level (g/dL)	43 [11] (10–13)
Prostate-specific antigen level (ng/mL)	43 [222] (69–1486)
Alkaline phosphatase level (IU/L)	43 [140] (88–586)
Lactate dehydrogenase level (IU/L)	43 [183] (151–247)
Albumin level (g/dL)	43 [37] (32–39)
BSI	32 [7.9] (2–11.5)
CTC count (cells per 7.5 mL of blood)	21 [35] (7–148)
Prior treatments‡	
Docetaxel	29 (67.4)
Cabazitaxel	10 (23.3)
Abiraterone acetate	27 (62.8)
Enzalutamide	7 (16.3)
Radium-223	1 (2.3)
Bisphosphonates	6 (14)
Palliative radiation therapy to bone	22 (51.2)
Sites of metastatic disease‡	
Bone only	20 (46.5)
Bone and nodal	17 (39.5)
Bone and viscera	6 (14)
Metastatic bone disease characteristics	
Median tDV (mL)§	503.1 (5.6–2242)
Median ADC (x10^{-6} mm^2/sec)‖	813 (780, 906)
Median OS (mo)‖	12.9 (8.7, 16.1)

* Unless otherwise specified, data are numbers of patients.

† Numbers in brackets are medians. Numbers in parentheses are the IQR.

‡ Numbers in parentheses are percentages.

§ Numbers in parentheses are the range.

‖ Numbers in parentheses are 95% CIs.

BSI Calculation

For those patients who underwent bone scintigraphy within 12 weeks of MR imaging and for whom Digital Imaging and Communication in Medicine images were available, the BSI was calculated by using an automated BSI scoring software system (Exini Diagnostics, Lund, Sweden) (22).

Statistical Analysis

The Pearson correlation coefficient (r) was determined to establish the correlation between variables. Kaplan-Meier analysis was used to study the OS of the population. Patients who were alive at the time of last follow-up were censored. Cox proportional hazards models were used to determine the association of the variables with OS. The comparison between the discriminative ability of MR imaging and bone scintigraphy in the prediction of OS was performed by assessing the status of each patient (dead vs alive) at several time points (9, 12, and 15 months) and determining the area under the receiver operating characteristic curve (concordance index, or C-index). Comparison between receiver operating characteristic curves was performed with the method established by DeLong et al (23). The 95% confidence interval (CI) of the median ADC of the entire population was calculated by means of bootstrapping. tDV, BSI, prostate-specific antigen level, CTC count, alkaline phosphate level, and lactate dehydrogenase level were log-transformed to account for the lack of normal distribution. The intra- and interobserver reliability of tDV measurements were assessed by using the Lin concordance correlation coefficient of absolute agreement and Bland-Altman analysis. Limits of agreement were defined as the mean difference ± 1.96 times the standard deviation of the differences. The coefficient of repeatability was calculated as 1.96 times the standard deviation of the differences between the two measurements. Software (SPSS, version 20; IBM, Armonk, NY) was used for statistical analyses.

Results

Forty-three patients were eligible and included in the analysis. Twenty of the 43 patients (46.5%) had metastatic disease limited to bone, 17 (39.5%) had bone and nodal disease, and six (14%) had visceral disease in addition to bone metastases.

Patients in our dataset had received a median of three (range, 0–7) lines of treatment for mCRPC at the time of MR imaging, including four patients (9.3%) who were treatment-naïve for mCRPC in whom MR imaging was performed within 4 weeks before their first systemic treatment for mCRPC. Twenty-eight of the 43 patients (65.1%) had undergone previous treatment with at least abiraterone acetate and/or enzalutamide and 29 (67.4%) were previously treated with taxane-based chemotherapy.

Thirty of the 43 patients (69.8%) died during the follow-up period, with 13 patients (30.2%) alive at the time of data analysis. The median OS of the overall population was 12.9 months (95% CI: 8.7, 16.1 months), with a median follow-up of 11.1 months (interquartile range [IQR]: 7.4–15.7 months). Patient and tumor characteristics, including treatment received before inclusion in our study, are summarized in Table 2.

The median tDV was 503.1 mL (range, 5.6–2242 mL), with a median global ADC for the regions of interest

Figure 3

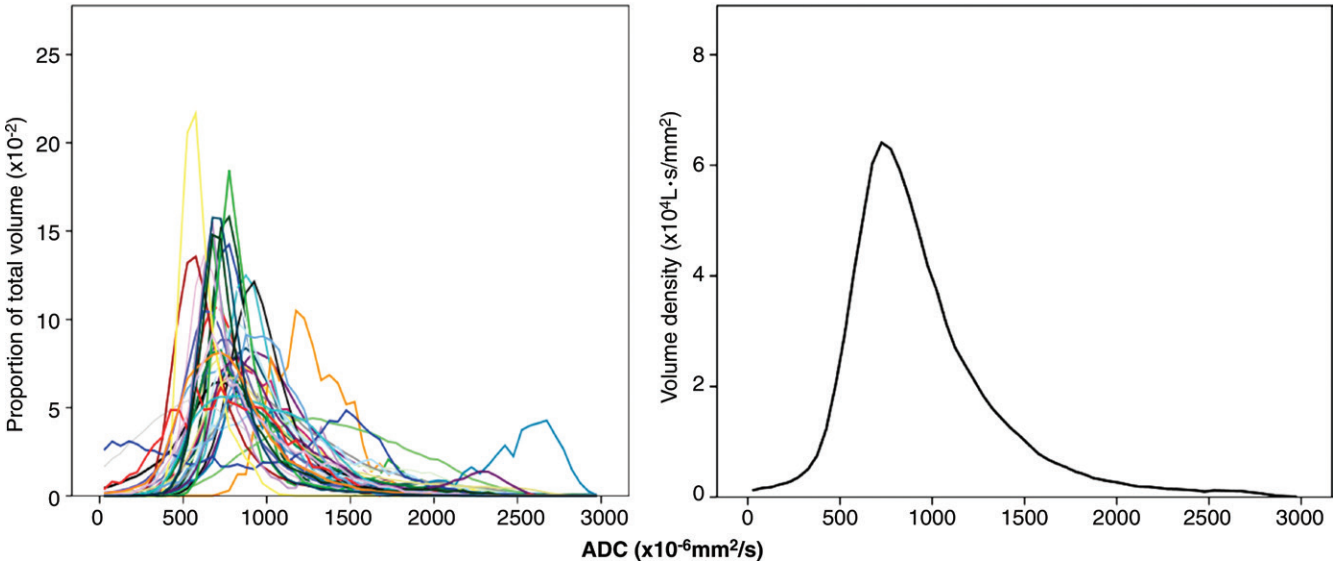

Figure 3: Left, histogram representation of ADCs for every patient included in analysis (n = 43). Right, volume density plot, where the y-axis represents the volume density per unit ADC. The area under the curve thus represents the total volume of disease in the patient population.

for each individual of 813 × 10^{-6} mm^2/sec (95% CI: 780, 906 × 10^{-6} mm^2/sec), median skewness of 1.5 (IQR: 0.9–1.9), and median kurtosis of 3.5 (IQR: 1.4–7). Histograms of the global ADCs for each patient and the whole population are shown in Figure 3. Two patients had bimodal histograms, with a high density of ADCs within 500–1500 × 10^{-6} mm^2/sec and a smaller peak within 2000–3000 × 10^{-6} mm^2/sec. Both cases corresponded to patients who received focal palliative radiation therapy to the pelvis during the 6 months before MR imaging (Fig 4).

Correlation of tDV with Prognostic Factors

We investigated the correlation between tDV and known established prognostic factors, with special interest in those associated with bone disease (eg, hemoglobin and alkaline phosphate levels). Overall, tDV showed a significant correlation with all of the studied established prognostic factors for mCRPC (hemoglobin level: $r = -0.521$, $P < .001$; prostate-specific antigen level: $r = 0.556$, $P < .001$; lactate dehydrogenase level: $r = 0.534$, $P < .001$; and alkaline phosphate level: $r = 0.572$, $P < .001$) (Table 3).

Next, we explored the correlation between tDV and CTC count. Baseline CTC counts were available for 21 of the 43 patients (48.8%). The median CTC count was 35 cells per 7.5 mL (IQR: 7–148 cells per 7.5 mL). CTC count showed significant correlation with tDV ($r = 0.613$, $P = .004$), which is consistent with published evidence that high CTC count informs on worse prognosis in mCRPC (24) (Fig 5).

Association of tDV with OS

We hypothesized that the burden of bone disease would associate with OS in patients with mCRPC; tDV, as a continuous variable, showed a statistically significant association with OS, with patients with a higher tDV having an increased risk of death (hazard ratio: 1.74; 95% CI: 1.02, 2.96; $P = .035$).

Association of Other Parameters Derived from Whole-Body DW Imaging with OS

Histogram parameters that describe the distribution of the global ADCs of bone metastases, such as mean (hazard ratio: 1; 95% CI: 0.998, 1.001; $P = .876$), median (hazard ratio: 1; 95% CI: 0.998, 1.002; $P = .928$), skewness (hazard ratio: 0.92; 95% CI: 0.563, 1.504; $P = .740$), or kurtosis (hazard ratio: 0.97; 95% CI: 0.89, 1.06; $P = .532$) did not show a significant association with OS in our population.

Comparison of the Predictive Ability of Whole-Body DW Imaging and BSI

Among the 43 patients, 32 (74.4%) had BSI data available for analysis from bone scans obtained within the prespecified time ranges. Seven of the 43 patients (16.3%) underwent bone scintigraphy more than 12 weeks apart from MR imaging and were therefore excluded from this subanalysis. Two of the 43 patients (4.7%) did not have results from bone scintigraphy available, and two (4.7%) did not have Digital Imaging and Communications in Medicine images, which are necessary for BSI calculation, available. The median BSI was 7.9 (IQR, 2–11.5). The tDV measured with whole-body DW imaging, as a continuous variable, and the estimation relative to total skeletal mass by the BSI were highly correlated ($r = 0.565$, $P = .001$) (Fig 5). To further assess the prognostic performance of BSI and tDV, we evaluated mortality rates at 9, 12, and 15 months (when approximately one-third, one-half, and two-thirds of patients had died). Receiver operating characteristic

Figure 4

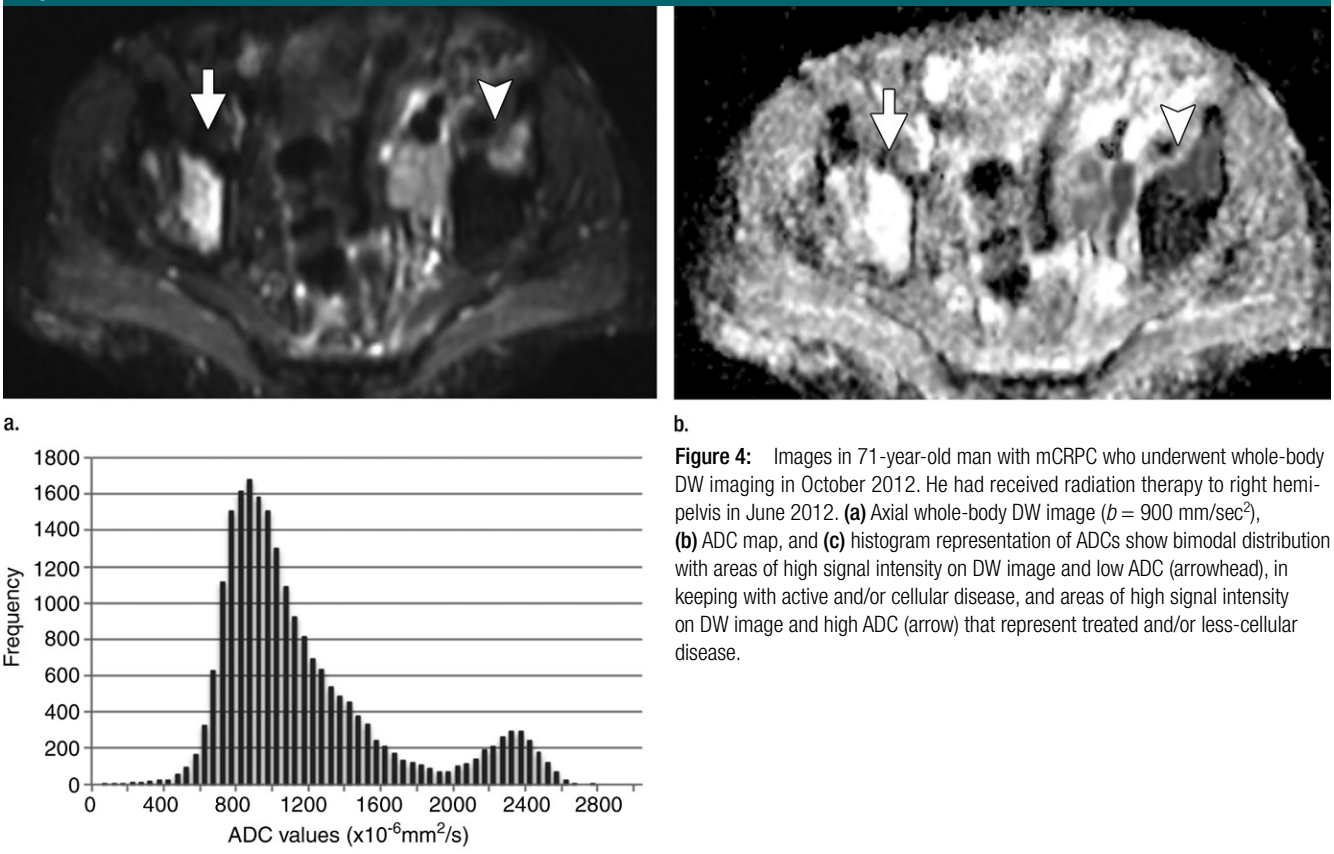

Figure 4: Images in 71-year-old man with mCRPC who underwent whole-body DW imaging in October 2012. He had received radiation therapy to right hemipelvis in June 2012. **(a)** Axial whole-body DW image (b = 900 mm/sec^2), **(b)** ADC map, and **(c)** histogram representation of ADCs show bimodal distribution with areas of high signal intensity on DW image and low ADC (arrowhead), in keeping with active and/or cellular disease, and areas of high signal intensity on DW image and high ADC (arrow) that represent treated and/or less-cellular disease.

Table 3

Correlation of tDV and Other Prognostic Factors

Prognostic Factor	Correlation Coefficient*	*P* Value
Hemoglobin level	−0.521	<.001
Prostate-specific antigen level	0.556	<.001
Lactate dehydrogenase level	0.534	<.001
Alkaline phosphatase level	0.572	<.001
Albumin level	−0.332	.030
CTC count	0.613	.004

Note.—The tDV, prostate-specific antigen level, lactate dehydrogenase level, alkaline phosphate level, and CTC count were log-transformed.

* Pearson correlation coefficient.

curve analysis was performed to determine the C-statistic (area under the receiver operating characteristic curve) with each of both imaging biomarkers at the specified time points. Although the area under the receiver operating characteristic curve for tDV was consistently superior to that for BSI for 9-month (0.745 vs 0.613, respectively; P = .141), 12-month (0.686 vs 0.627; P = .533), and 15-month (0.704 vs 0.607; P = .345) mortality rates (Fig E1 [online]), these differences were not statistically significant.

Intra- and Interobserver Reliability of tDV Measurement

The intraclass correlation coefficients were 0.986 (95% CI: 0.945, 0.996) and 0.949 (95% CI: 0.857, 0.981) for intra- and interobserver comparison, respectively. The Bland-Altman–calculated intraobserver coefficient of repeatability was 0.302 L, and the interobserver coefficient of repeatability was 0.500 L. All values in the intra- and interobserver Bland-Altman analysis are within the 95% limits of agreement.

Discussion

Bone involvement in patients with advanced prostate cancer is extremely common, resulting in higher morbidity and mortality in patients with mCRPC. When we consider the limitations of CT and bone scintigraphy in the accurate assessment of the extent of bone metastases, it is imperative to develop new imaging biomarkers and pursue their analytical and clinical quantification, with the aim of providing new tools for guiding radiologists and clinicians in therapeutic decisions.

Our study shows an association between whole-body DW imaging parameters, OS, and prognostic factors in mCRPC, which was previously

Figure 5

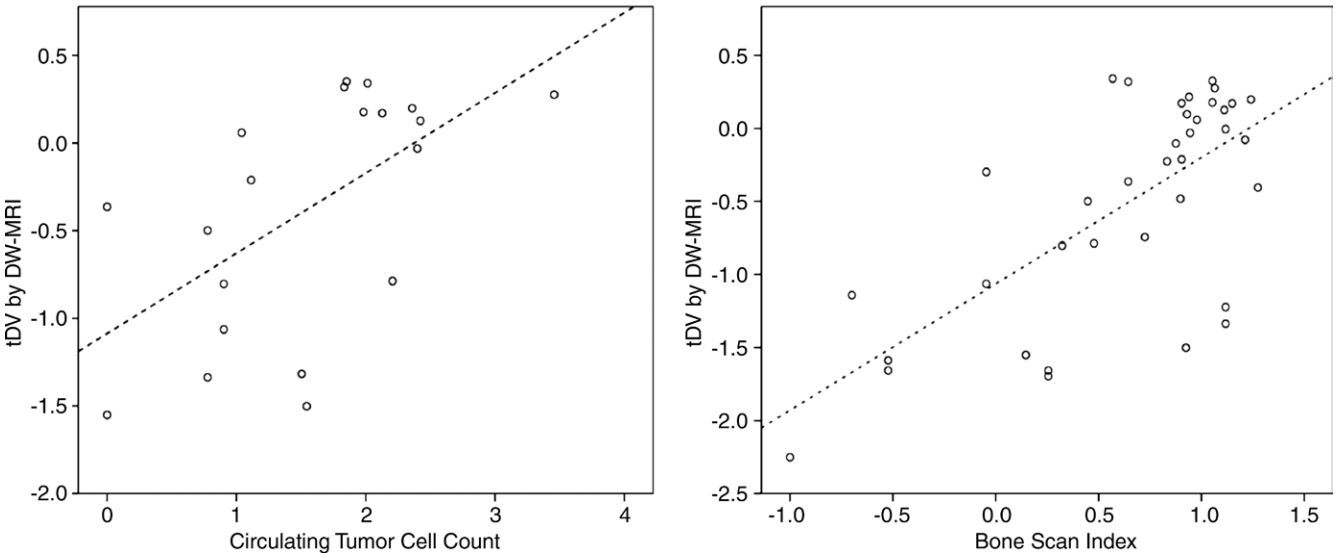

Figure 5: Scatterplots show relationship between tDV and CTC count and between tDV and BSI.

established in the literature. Notably, the volume of bone metastasis quantified with whole-body DW imaging correlates with prognostic biomarkers routinely implemented into standard physician's practice, such as hemoglobin level, prostate-specific antigen level, and the bone turnover marker alkaline phosphate level. Interestingly, we also detected a correlation with CTC count, an established prognostic biomarker in mCRPC, although these findings must be corroborated in larger populations.

Histogram representation of the ADCs of the burden of metastatic bone disease may also provide a useful representation of tissue cellularity. The median ADC for our population was 813 × 10^{-6} mm^2/sec; this value is lower than the median ADC reported in previous studies in other tumor types, including multiple myeloma (25), a disease with predominately lytic disease. In this mCRPC population, conversely, metastases were mainly sclerotic (26). Studies in which DW imaging is used as a biomarker in cancer medicine, therefore, must account for such differences in disease biology among tumor types. Furthermore, bimodal histograms reflect the coexistence of two different patterns of disease with different cellular density distributions (27).

Parameters that help describe the distribution of the global ADCs of bone metastases, such as mean, median, skewness, or kurtosis, were not associated with OS in our population.

In the past few years it has been shown that indirect measurements of the burden of bone metastases, measured either as proportion of skeletal mass with BSI or the number of lesions visible at CT and PET/CT, provide prognostic information in prostate cancer (28,29). These examinations, however, only largely reflect bone turnover as a response to either benign or malignant processes. MR imaging has been previously shown to have higher sensitivity and specificity than bone scintigraphy and CT in the detection of bone metastases (12). In our data set, the receiver operating characteristic curves with bone scintigraphy were consistently inferior to those with whole-body DW imaging in the prediction of mortality, which suggests that the performance of DW imaging is superior. However, considering the limited population included in our study, formal comparisons in larger cohorts will be necessary to confirm this finding because the differences did not reach statistical significance.

We acknowledge the potential limitations of our study. First, the retrospective observational nature of our work, the variability in the number and type of treatments administered in the time between MR imaging and the start of therapy, and the presence of nodal and visceral disease in some of our patients are limitations. Second, because of the limited sample size of our pilot study, it is important to note that we did not control for clinical factors in the evaluation of the association between tDV and OS. A larger population would be needed for future validation of these data, allowing for multivariate analysis—ideally in the setting of prospective studies. Third, there is a risk of underestimating the disease because the presented data included skeletal segmentation from the cervical spine to midthighs only. However, taking into account that the vast majority of bone metastases occur within the spine and pelvis (20), it is unlikely that this had a major effect on the assessment of the total burden of metastatic bone disease. Finally, it should be noted that delineation of the volume of interest is dependent on the quality of the acquired DW imaging data, the

semiautomatic segmentation tool, and radiologist expertise. Despite these limitations, to our knowledge, our study represents the largest series assessing mCRPC bone metastasis with DW imaging and the data presented herein support further evaluation of whole-body DW imaging in this disease.

One practical conclusion of our study is the demonstration of the feasibility of assessing metastatic bone disease from prostate cancer with whole-body DW imaging; indeed, in 49 of 53 cases reviewed (92%) the outcome of DW imaging was fully suitable for assessment. We are currently able to perform whole-body DW imaging in reasonably short data acquisition times (24 minutes), thus analyzing whole-tumor burden and its spatial heterogeneity. Other advantages of whole-body MR imaging including DW imaging compared with the current standard of CT and bone scintigraphy are the avoidance of the need for radiation or radioactive materials, evaluation of both soft-tissue and bone metastases, and accurate depiction of complications such as cord compression or bone fractures. Whole-body MR imaging including DW imaging can be implemented in everyday clinical practice, as the technique is robust and the protocols can be implemented in most of the commonly used imaging units.

In conclusion, we have shown a strong correlation between tDV assessed with whole-body DW imaging and proved prognostic factors in mCRPC, including CTC counts, and present promising data that support an association between tDV and OS. Our results, taken together with those from previous reports that describe changes in DW imaging after exposure to anticancer treatments (30), raise the need for further evaluation of DW imaging as a prognostic and response biomarker in prospective cohorts of patients with mCRPC to acquire clinical qualification and, eventually, implementation in routine clinical practice.

Acknowledgments: This study was supported by Prostate Cancer UK and the Stand Up To Cancer–Prostate Cancer Foundation Prostate Dream Team Translational Cancer Research Grant; Stand Up To Cancer is a program of the Entertainment Industry Foundation administered by the American Association for Cancer Research (SU2C-AACR-DT0712). Raquel Perez-Lopez conducted this work in the Medicine Doctorate framework of the Universidad Autonoma de Barcelona. The authors thank other clinical research fellows at the Prostate Cancer Targeted Therapy Group and radiographers at The Royal Marsden NHS Foundation Trust and the Institute of Cancer Research. We acknowledge patients and their families for their collaboration toward research.

Disclosures of Conflicts of Interest: R.P. disclosed no relevant relationships. **D.L.** Activities related to the present article: disclosed no relevant relationships. Activities not related to the present article: receives consulting fees from Sanofi. Other relationships: disclosed no relevant relationships. **M.D.B.** disclosed no relevant relationships. **D.J.C.** disclosed no relevant relationships. **J.M.** disclosed no relevant relationships. **D.B.** disclosed no relevant relationships. **A.O.** disclosed no relevant relationships. **A.Z.** disclosed no relevant relationships. **M.O.L.** disclosed no relevant relationships. **J.S.d.B.** disclosed no relevant relationships. **D.M.K.** disclosed no relevant relationships. **N.T.** disclosed no relevant relationships.

References

1. Ferlay J, Soerjomataram I, Dikshit R, et al. Cancer incidence and mortality worldwide: sources, methods and major patterns in GLOBOCAN 2012. Int J Cancer 2015;136(5):E359–E386.
2. Gandaglia G, Abdollah F, Schiffmann J, et al. Distribution of metastatic sites in patients with prostate cancer: a population-based analysis. Prostate 2014;74(2):210–216.
3. Carlin BI, Andriole GL. The natural history, skeletal complications, and management of bone metastases in patients with prostate carcinoma. Cancer 2000;88(12 Suppl):2989–2994.
4. Saad F, Lipton A, Cook R, Chen YM, Smith M, Coleman R. Pathologic fractures correlate with reduced survival in patients with malignant bone disease. Cancer 2007;110(8):1860–1867.
5. Sathiakumar N, Delzell E, Morrisey MA, et al. Mortality following bone metastasis and skeletal-related events among men with prostate cancer: a population-based analysis of US Medicare beneficiaries, 1999–2006. Prostate Cancer Prostatic Dis 2011;14(2):177–183.
6. de Bono JS, Logothetis CJ, Molina A, et al. Abiraterone and increased survival in metastatic prostate cancer. N Engl J Med 2011;364(21):1995–2005.
7. Scher HI, Fizazi K, Saad F, et al. Increased survival with enzalutamide in prostate cancer after chemotherapy. N Engl J Med 2012;367(13):1187–1197.
8. Shen G, Deng H, Hu S, Jia Z. Comparison of choline–PET/CT, MRI, SPECT, and bone scintigraphy in the diagnosis of bone metastases in patients with prostate cancer: a meta-analysis. Skeletal Radiol 2014;43(11):1503–1513.
9. Jambor I, Kuisma A, Ramadan S, et al. Prospective evaluation of planar bone scintigraphy, SPECT, SPECT/CT, (18)F-NaF PET/CT and whole body 1.5T MRI, including DWI, for the detection of bone metastases in high risk breast and prostate cancer patients: SKELETA clinical trial. Acta Oncol 2016;55(1):59–67.
10. Koh DM, Collins DJ. Diffusion-weighted MRI in the body: applications and challenges in oncology. AJR Am J Roentgenol 2007;188(6):1622–1635.
11. Luboldt W, Küfer R, Blumstein N, et al. Prostate carcinoma: diffusion-weighted imaging as potential alternative to conventional MR and 11C-choline PET/CT for detection of bone metastases. Radiology 2008;249(3):1017–1025.
12. Lecouvet FE, El Mouedden J, Collette L, et al. Can whole-body magnetic resonance imaging with diffusion-weighted imaging replace Tc 99m bone scanning and computed tomography for single-step detection of metastases in patients with high-risk prostate cancer? Eur Urol 2012;62(1):68–75.
13. Guo AC, Cummings TJ, Dash RC, Provenzale JM. Lymphomas and high-grade astrocytomas: comparison of water diffusibility and histologic characteristics. Radiology 2002;224(1):177–183.
14. Hayashida Y, Hirai T, Morishita S, et al. Diffusion-weighted imaging of metastatic brain tumors: comparison with histologic type and tumor cellularity. AJNR Am J Neuroradiol 2006;27(7):1419–1425.
15. Zelhof B, Pickles M, Liney G, et al. Correlation of diffusion-weighted magnetic resonance data with cellularity in prostate cancer. BJU Int 2009;103(7):883–888.
16. Liu Y, Ye Z, Sun H, Bai R. Clinical application of diffusion-weighted magnetic resonance imaging in uterine cervical cancer. Int J Gynecol Cancer 2015;25(6):1073–1078.
17. Matsubayashi RN, Fujii T, Yasumori K, Muranaka T, Momosaki S. Apparent diffusion coefficient in invasive ductal breast carcinoma: correlation with detailed histologic features and the enhancement ratio on dynamic contrast-enhanced MR images. J Oncol doi: 10.1155/2010/821048. Published online September 2, 2010. Accessed April 15, 2015.

18. Oken MM, Creech RH, Tormey DC, et al. Toxicity and response criteria of the Eastern Cooperative Oncology Group. Am J Clin Oncol 1982;5(6):649–655.

19. Olmos D, Arkenau HT, Ang JE, et al. Circulating tumour cell (CTC) counts as intermediate end points in castration-resistant prostate cancer (CRPC): a single-centre experience. Ann Oncol 2009;20(1):27–33.

20. Kakhki VR, Anvari K, Sadeghi R, Mahmoudian AS, Torabian-Kakhki M. Pattern and distribution of bone metastases in common malignant tumors. Nucl Med Rev Cent East Eur 2013;16(2):66–69.

21. Kraan J, Sleijfer S, Strijbos MH, et al. External quality assurance of circulating tumor cell enumeration using the CellSearch(®) system: a feasibility study. Cytometry B Clin Cytom 2011;80(2):112–118.

22. Ulmert D, Kaboteh R, Fox JJ, et al. A novel automated platform for quantifying the extent of skeletal tumour involvement in prostate cancer patients using the bone scan index. Eur Urol 2012;62(1):78–84.

23. DeLong ER, DeLong DM, Clarke-Pearson DL. Comparing the areas under two or more correlated receiver operating characteristic curves: a nonparametric approach. Biometrics 1988;44(3):837–845.

24. de Bono JS, Scher HI, Montgomery RB, et al. Circulating tumor cells predict survival benefit from treatment in metastatic castration-resistant prostate cancer. Clin Cancer Res 2008;14(19):6302–6309.

25. Messiou C, Collins DJ, Morgan VA, Desouza NM. Optimising diffusion-weighted MRI for imaging metastatic and myeloma bone disease and assessing reproducibility. Eur Radiol 2011;21(8):1713–1718.

26. Messiou C, Collins DJ, Morgan VA, Bianchini D, de Bono JS, de Souza NM. Use of apparent diffusion coefficient as a response biomarker in bone: effect of developing sclerosis on quantified values. Skeletal Radiol 2014;43(2):205–208.

27. Padhani AR, van Ree K, Collins DJ, D'Sa S, Makris A. Assessing the relation between bone marrow signal intensity and apparent diffusion coefficient in diffusion-weighted MRI. AJR Am J Roentgenol 2013;200(1):163–170.

28. Kaboteh R, Damber JE, Gjertsson P, et al. Bone scan index: a prognostic imaging biomarker for high-risk prostate cancer patients receiving primary hormonal therapy. EJNMMI Res 2013;3(1):9.

29. Vargas HA, Wassberg C, Fox JJ, et al. Bone metastases in castration-resistant prostate cancer: associations between morphologic CT patterns, glycolytic activity, and androgen receptor expression on PET and overall survival. Radiology 2014;271(1):220–229.

30. Blackledge MD, Collins DJ, Tunariu N, et al. Assessment of treatment response by total tumor volume and global apparent diffusion coefficient using diffusion-weighted MRI in patients with metastatic bone disease: a feasibility study. PLoS One 2014;9(4):e91779.